Soft Matter

The effect of cisplatin on the nanoscale structure of aqueous PEO-PPO-PEO micelles of varying hydrophilicity observed using SAXS

SCHOLARONE™
Manuscripts

1   Title: The effect of cisplatin on the nanoscale structure of aqueous PEO-PPO-PEO micelles of
2   varying hydrophilicity observed using SAXS
3
4   Andre L. Thompson;[a] Lydia M. Mensah[a] Brian J. Love[a,b,*]
5
6   [a]Department of Materials Science and Engineering
7   University of Michigan
8   2644 Bob and Betty Beyster Bldg
9   Ann Arbor, MI, USA 48109
10
11   [b]Department of Biomedical Engineering,
12   University of Michigan
13   Ann Arbor, MI, USA 48109
14
15   *Corresponding Author
16   Email: bjlove@umich.edu
17   Phone: 1-734-763-2013
18   FAX:734-763-4788
19   Cell 734-478-8101

20   **Abstract:**
21

22   Aqueous solutions of polyethylene oxide-polypropylene oxide-polyethylene oxide (PEO-PPO-
23   PEO) copolymers form micelles and cubic lattices as their temperature is raised. The presence of
24   added solutes within the dispersions can also affect the kinetics of structure formation. Here, we
25   investigate the structures formed in the amphiphiles P104, P105, and F108 solutions at 31%
26   mass/v both neat and co-formulated with the drug cisplatin (0.02% to 0.1% mass/v) using small-
27   angle X-ray scattering. P104 formed BCC colloidal crystals while P105 and F108 formed FCC
28   structures. Cisplatin had a minor influence of the formation and stability of the crystals during
29   these thermal excursions. The largest interaction between the amphiphiles and cisplatin was
30   P104 where there was a 2% reduction in the BCC lattice parameter of P104 as cisplatin loading
31   rose to 0.1% at 28°C. The F108 unit cell swelled ~2% upon cisplatin loading of 0.1%. A
32   progressive evolution and breakdown of these structures was noted as temperature rose from
33   10°C to 35°C. For the different amphiphiles, crystal thermal expansion coefficients of ~1×10^{-2}/°C
34   were determined in neat and loaded amphiphiles with cisplatin and all the crystals swelled with
35   increasing temperature.
36
37
38
39   **Keywords**: micelle, cisplatin, SAXS, Pluronic F108, P105, P104
40

1. **Introduction**:

Scientists have previously probed temperature-dependent micellization and ordering of PEO-PPO-PEO triblock copolymers in aqueous solutions[1-11]. As the temperature of these solutions rise, the decreasing aqueous solubility of the PPO segments forms micelles from hydrophobic (PPO) cores and hydrophilic (PEO) tail blocks forming shells [8]. Lam et al suggested micelles grow via Ostwald ripening [10] and Barba et al suggested that the volume fraction occupied by the micelles in solution rises with increasing temperature [11]. At high concentration, the micelles experience repulsive interactions and order into quasicrystalline cubic lattices leading to their gel-like properties [8]. Micellization and ordering are reversible as there is no irreversible chemical cross-linking of the polymer chains [8].

Biomedical researchers are interested in this reversible temperature-dependent gelation behavior because one can use ambient metabolic heating to trigger gelation if the gel temperatures of these amphiphiles is sufficiently low[12-16]. These solutions can be injected cold, and then gel *in situ* as the solution warms to body temperature [8]. The rigidity of the gel allows one to inject drug infused copolymers; the gels that form regulate the localized permeation of added pharmaceuticals, which might lead to a more sustained delivery and longer local residence time [16].

It is known that ternary additives can influence the aqueous micellization and gelation behavior of PEO-PPO-PEO amphiphiles[8, 9, 17]. Methylparaben, for example, lowers the gelation temperature of the amphiphile F127 solution by as much as $10\text{-}15^{\circ}C$[5, 9]. A structural evaluation is important to understand the structure-property relationship that exists in these pharmaceutical-loaded amphiphile formulations.

64   We've been considering a compound with the tradename cisplatin, an effective

65   chemotherapeutic of relatively low aqueous solubility. There are suggestions that packaging

66   cisplatin within a surfactant could raise both its solubility and the ability to sustain a dose

67   locally. We previously probed how cisplatin affects the PEO-PPO-PEO micelle formation in the

68   low concentration regime to identify a critical micelle concentration and at higher concentrations

69   co-formulated with cisplatin [18]. We proposed that the enthalpy-entropy compensation plots for

70   neat and cisplatin-loaded solutions of amphiphilic copolymers can resolve the perturbation in the

71   micelle formation energetics due to the additive, and an indicator of surfactant quality in

72   formulated dispersions coerced into directed assembly [18]. $T_{compensation}$ was essentially invariant

73   adding cisplatin to the highly hydrophobic copolymer L101, the hydrophilic copolymer F108,

74   and the more amphiphilic copolymer P105, but cisplatin had a profound effect on the more

75   amphiphilic P104 [18].

76   Small angle X-ray and Neutron scattering (SAXS and SANS) have been used previously

77   to study the structure and organization of micellar systems [19-22, 8], including P104 [23-35],

78   P105 [36-41], and F108 [42-50]. These techniques allow insight into both the structures within

79   the micelles and also the lattice structures into which they arrange. Svensson et al noticed SAXS

80   diffraction patterns for P104 in the normal micellar liquid crystalline phase, I1, composition 31%

81   mass v^{-1} at 25°C [29]. Using DSC, we also noticed that the micellization endotherm in P104 was

82   influenced by adding cisplatin which must migrate to the core/shell interface between the

83   hydrophobic and hydrophilic regions of the micelle [18]. Here, we use SAXS to investigate

84   crystal formations of P104, P105, and F108 solutions as they are heated through their gelation

85   temperatures. Our aim was to identify changes in quasicrystalline lattice formation as an effect of

86   added cisplatin, and resolve whether it is located within the micelles' core, shell, core/shell

87   interface, or randomly dispersed in solution. We observed the structural changes associated with

88   the presence of cisplatin on P104, P105, and F108 and examined the different kinetics of gel

89   formation with varying core-shell dimension. With the complications for therapeutic delivery

90   linked with the limited solubility of hydrophobic drugs, key features in bioavailability could be

91   linked to the thermodynamic mixing of drug/amphiphile combinations.

92
93   **2. Materials and Methods**:
94
95   **Solution Preparation.** Pluronics P104, P105, and F108 were obtained from BASF

96   (Wyandotte, MI) and used as received. Aqueous solutions of 31% mass v^{-1} P104, P105, and

97   F108 were each prepared according to the "cold" processing method of Schmolka[51] by

98   dissolving weighed amounts of each amphiphile into distilled water, which were then left to

99   solubilize quiescently at 4°C. At this high concentration, repeated cool/mix cycles were needed

100   to fully solubilize the polymers. Cis-diaminedichloroplatinum(ii) (MW= 298g/mol), known by

101   the trade name cisplatin (Sigma-Aldrich), was used as received and added to aqueous solutions

102   of these varying Pluronics®(P104, P105, F108).

103   Amphiphilic PEO-PPO-PEO micelle structures can be produced in which both the overall

104   chain length and relative amount of hydrophobic to hydrophilic blocks can be regulated. The

105   block copolymers are cross-referenced based on a XXY designation where XX corresponds to

106   the length of the PPO block. Multiplying this number by 300 gives the approximate molecular

107   weight of the PPO center block. The Y corresponds to the mass fraction (as 1/10 the weight

108   percentage) of the molecule that is comprised of PEO hydrophilic blocks, as indicated in a prior

109   publicaiton [18]. So Pluronic ® F108 has a molecular mass of ~ 15,KDa, a PPO block of 3KDa

110   and 80% of the block lengths are hydrophilic. Block copolymers of a similar overall length and

111   longer hydrophobic blocks reduce Y from 8 to a lower number. Two types of formulation

112 protocols were followed. One fixed each Pluronic (P104, P105, and F108) content and cisplatin

113 content at 31% mass v^{-1} and 0.1% mass v^{-1} respectively, to investigate the structures formed in

114 both neat and co-formulated with cisplatin to study both the progressive evolution and

115 breakdown of these structures as the temperature is increased from 10°C to 35°C. We also fixed

116 P104 (31% mass v^{-1}) and varied the cisplatin concentrations from 0.02% to 0.1% mass v^{-1} in

117 0.02% increments as solutions were heated through 10°C to 35°C.

118 **Small-Angle X-ray Scattering.** SAXS experiments were conducted at Argonne National

119 Laboratory (Argonne, IL) at the Advanced Photon Source (APS) on beamline 12-BM-B

120 operating at 12 keV. Static heating tests resolved the structure as the temperature rose from 10°C

121 and 35°C. Each sample was aliquoted into thin-walled capillary tubes (0.01 mm wall thickness)

122 and simultaneously placed into the heating stage while exposed to the X-ray source. Each sample

123 was subjected to a 1-minute equilibration time at 10°C to ensure the sample temperature was

124 uniform and steady. Scattering data was collected for each sample for 1 minute. After data

125 collection, the heating stage ramped up 2°C, followed by another 1-minute equilibration, then re-

126 exposed again for 1 minute. This process was repeated until 34°C was reached. During the

127 heating and equilibration phases, the X-ray shutters were closed. The starting and final

128 temperatures were chosen to be well below and above the gelation temperature of the sample,

129 respectively from prior determinations of the critical micelle concentrations of P104, P105, and

130 F108 using DSC [17, 18].

131 **Data Collection and Analysis.** 2D SAXS data were collected. The data was integrated

132 around the azimuthal axis to generate 1D plots of the measured intensity as a function of the

133 scattering vector q using SASView. These plots underwent a 9 point smoothing routine to reduce

134 noise. Peak positions in the generated I(q) plots were quantified using OriginLab's peak

135   analyzer function. These peaks were then compared to the expected reflections for the various

136   known crystal structures in order to identify the structures present in the solution. Table 1

137   presents a summary of the first five peaks and their positions relative to the fundamental

138   scattering peak for the FCC and BCC crystal systems [8].

139   **Table 1. Summary of expected peaks and relative peak positions for the BCC and FCC**
140   **crystals**

Crystal	q_0	q_1	q_2	q_3	q_4
bcc	(110)	(200)	(211)	(220)	(310)
position	q_0	$2^{1/2} q_0$	$3^{1/2} q_0$	$4^{1/2} q_0$	$5^{1/2} q_0$
fcc	(111)	(200)	(220)	(311)	(222)
position	q_0	$(4/3)^{1/2}q_0$	$(8/3)^{1/2} q_0$	$(11/3)^{1/2}q_0$	$(12/3)^{1/2}q_0$

141

142   The cubic lattice parameter a, can be obtained by plotting $(q/2\pi)^2$ (q is the scattering vector)

143   versus the sum of the Miller indices $(h^2 + k^2 + l^2)$ for each reflection, according to equation

144   (1)[34].

$$(q/2\pi)^2 = (1/a)^2(h^2 + k^2 + l^2)\tag{1}$$

146   At the APS beamline 12-BM-B, 12 keV of beam energy was used allowing us to solve for

147   frequency, v, in equation (2).

$$E = hv\tag{2}$$

149   Where E is energy of the beam and h is Planck's constant. Using frequency, v, and speed of light,

150   c, equation (3) can be used to solve for the wavelength, λ, of the X-rays.

$$\lambda = \frac{c}{v}\tag{3}$$

152   The relationship between q and theta for SAXS is identified in equation (4) where 2θ is the angle

153   between the incident X-ray beam and the detector measuring the scattering intensity.

$$q = \frac{4\pi \sin(\theta)}{\lambda} \tag{4}$$

155   Using Bragg's law, equation (5) can be used to solve for the spacing, d, between adjacent (hkl)

156   lattice planes.

$$d = \frac{\lambda}{2\sin(\theta)} \tag{5}$$

158   Finally, using the interplanar spacing, d, for cubic crystals as length, L, and the change in

159   temperature, ΔT, assuming negligible effect of pressure, the linear thermal expansion coefficient,

160   α_L, can be calculated with equation (6).

$$\alpha_L = \frac{\Delta L}{L \Delta T} \tag{6}$$

162   where L is the original length of the interplanar spacing, and $\Delta L / \Delta T$ is the rate of change of the

163   linear dimension per unit change in temperature.

164   **3. Results and Discussion**:

165

166   **Phase Structure Identification.** Figure 1 compares the presence of ordered phases for neat

167   P104 (31% mass v^{-1}) and P104 mixed cisplatin (0.1% mass v^{-1}) at 28°C with peak identifications.

168   Crystal structures were determined based on their ratio to the fundamental peak. A full list of

169   peak positions and phase structure for neat P104 (31% mass v^{-1}) and cisplatin mixed P104

170   (0.02%-0.1% mass v^{-1}) at 28°C is listed in Table 2. We are focused primarily on the structure

171   factor for this analysis, as it is well documented that these amphiphilic copolymer form spherical

172   micelles that could be interpreted either as core-shell structures or as hard spheres. The presence

173   of the small molecule cisplatin isn't large enough to organize a different form factor from these

174   micelles in solution. By confirming the separation of the scattering peaks, we can resolve

175   between different crystal structures

176
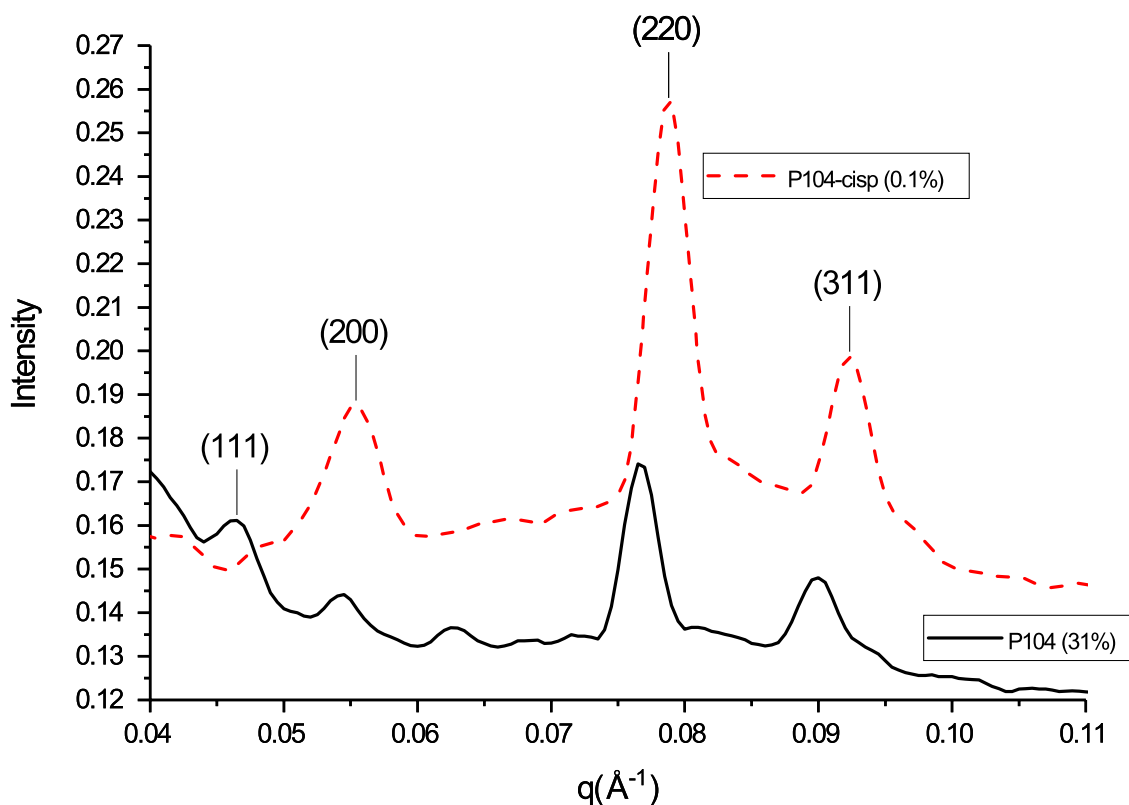
Figure 1. Comparison of peak identifications of neat P104 (31% mass v^{-1}) and P104 mixed cisplatin (0.1% mass v^{-1}) at 28°C.

Upon analyzing neat P104 at 28°C, it appears the primary peak, (111) at q_0, is suppressed

with added cisplatin, while preserving the higher order peaks. The higher order peaks are also

enhanced with added cisplatin, evidenced by a sharp rise in the signal to noise ratio. For

example, for the FCC peak (220) at $(4/3)^{1/2}q_0$ for neat P104, the intensity increased from

0.13:0.18, while with added cisplatin, the intensity for the same peak increased from 0.16:0.26.

This suggests cisplatin either enhances the structural ordering of the FCC crystals in P104 or the

platinum atom in cisplatin, itself a strong scatterer, and its co-location in organized

micelles enhances the coherence of the scattering. Since the higher order peaks are enhanced and

no broad scattering is observed once cisplatin is added, cisplatin is presumed to be mostly

located within the micelle and not randomly distributed in solution. This adds further evidence to

our previous claim (using DSC) that the moderately hydrophilic cisplatin interacts with the

191   micelle energetics [18]. There are also slight shifts to higher q values for p104 after adding

192   cisplatin (Table 2); the lattice plane spacing is reduced.

193   Cisplatin's inclusion was mostly invariant to the temperature at which ordering occurred

194   relative to neat P104 samples. Figure 2a and 2b shows stack plots of the neat P104 (a) vs 0.1%

195   cisplatin loaded P104 (b) as the temperature swept from 15-35°C. The crystal structures that

196   form are the same, but is a more pronounced scattering when cisplatin is included. The peaks

197   shift to lower q with increasing temperature indicative of swelling and the structures are lost by

198   the time the temperature is 35°C.   Coherent scattering was first seen when neat specimens of

199   neat P104 were heated to 20°C and was observed at 17°C-20°C for the cisplatin mixed P104

200   samples. Neat P104 ordered phases were slightly less stable. The FCC phase is clearly present up

201   to 28°C in neat specimens, and the peaks are lost at the next temperature interval. These are

202   clearly maintained in the cisplatin loaded specimens at 30°C but disappear at the next higher

203   temperature measurement. Preserving ordered phases at higher temperatures was also observed

204   by adding methylparaben and dexamethasone in F127 gels [8].
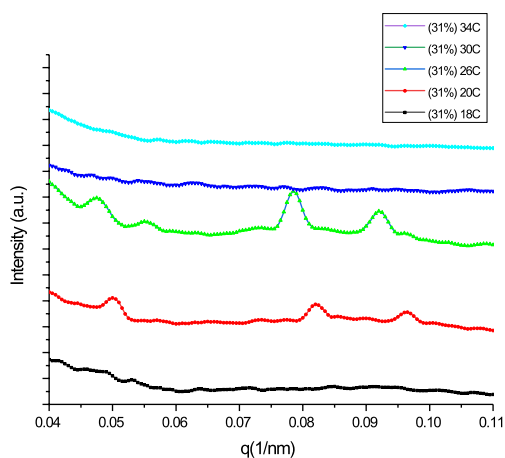
205

206   **Figure 2a**: . Representative stacked SAXS plots for neat 31% mas v^{-1} P104 solutions as the
207   temperature was swept from 15-35°C

208
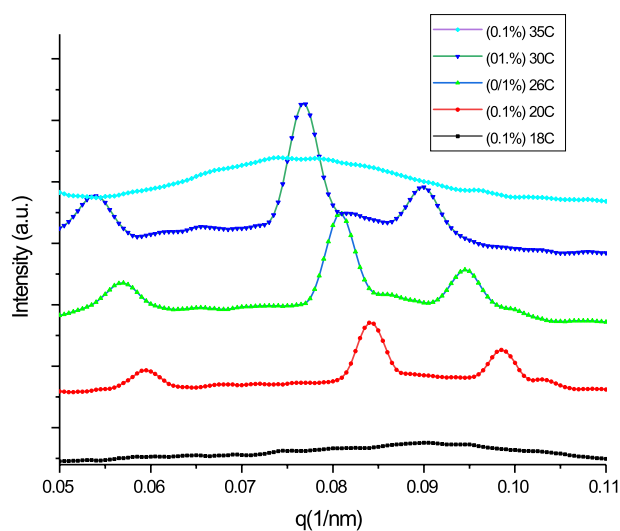
209

210   **Figure 2b**. Representative stacked SAXS plots of 0.1% mass v^{-1} cisplatin loaded 31% mass v^{-1}

211   P104 solutions as the temperature was swept from 15-35°C

212   Figure 3 compares the presence of ordered phases for neat P105 (31% mass v^{-1}) and P105

213   mixed cisplatin (0.1% mass v^{-1}) at 28°C with peak identifications. A full list of peak positions

214   and phase structure for neat P105 (31% mass v^{-1}) and cisplatin mixed P105 (0.1% mass v^{-1}) at

215   28°C is listed in Table 2. The scattering pattern is consistent with a BCC structure.

216
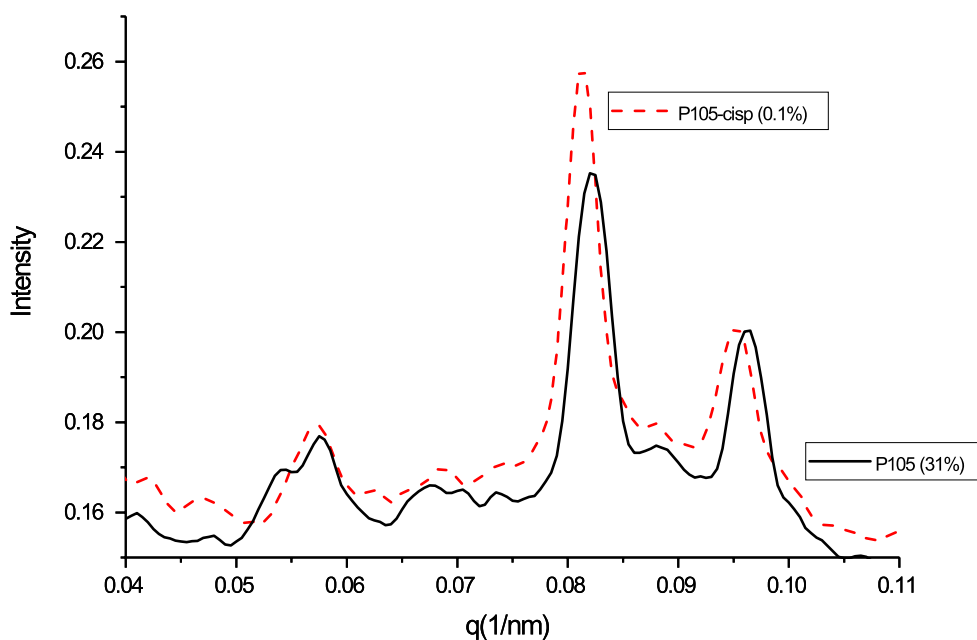
Figure 3. Comparison of peak identifications of neat P105 (31% mass v^{-1}) and P105 mixed
cisplatin (0.1% mass v^{-1}) at 28°C.

219

For cisplatin mixed P105 at 28°C, the primary peak, (110) at q_0, is seen, but only the bcc

peak (211) at $3^{1/2}q_0$ was enhanced (increase from 0.16:0.23 to 0.17:0.26) adding cisplatin. The

bcc peak (200) at $2^{1/2}q_0$ is also more defined with added cisplatin suggesting cisplatin enhances

the structural ordering of the BCC phases in P105 and the phases are stable. Since the higher

order peaks are enhanced and no random scattering is observed once cisplatin is added, this also

indicates cisplatin is situated mostly within micelles and not randomly distributed in solution.

There is a slight shift to lower q values with added cisplatin (Table 2), which indicates cisplatin

swells P105.

Similar to P104, the presence of cisplatin had little effect on the temperature where

ordering occurred relative to neat P105 samples. For example, an ordered phase was first seen in

the 18°C measurement for neat P105 as compared to 20°C measurement for the cisplatin mixed

231   P105 samples. Breakdown of the ordered phases was also evident at higher temperatures for neat

232   P105 as the bcc phase with the highest intensity was at 28°C, and decreased at 30°C; random

233   scattering was seen at 34°C. For cisplatin mixed P105, however, the highest intensity was seen at

234   30°C, again with random scattering at 34°C. Cisplatin stabilized the quasicrystalline lattice in

235   P105 gels slightly.

236   Figure 4 compares the presence of ordered phases for neat F108 (31% mass v^{-1}) and F108 mixed

237   cisplatin (0.1% mass v^{-1}) at 28°C with peak identifications for a BCC crystal. A full list of peak

238   positions and phase structure for neat F108 (31% mass v^{-1}) and cisplatin mixed F108 (0.1% mass

239   v^{-1}) at 28°C (both BCC structures) is listed in Table 2.
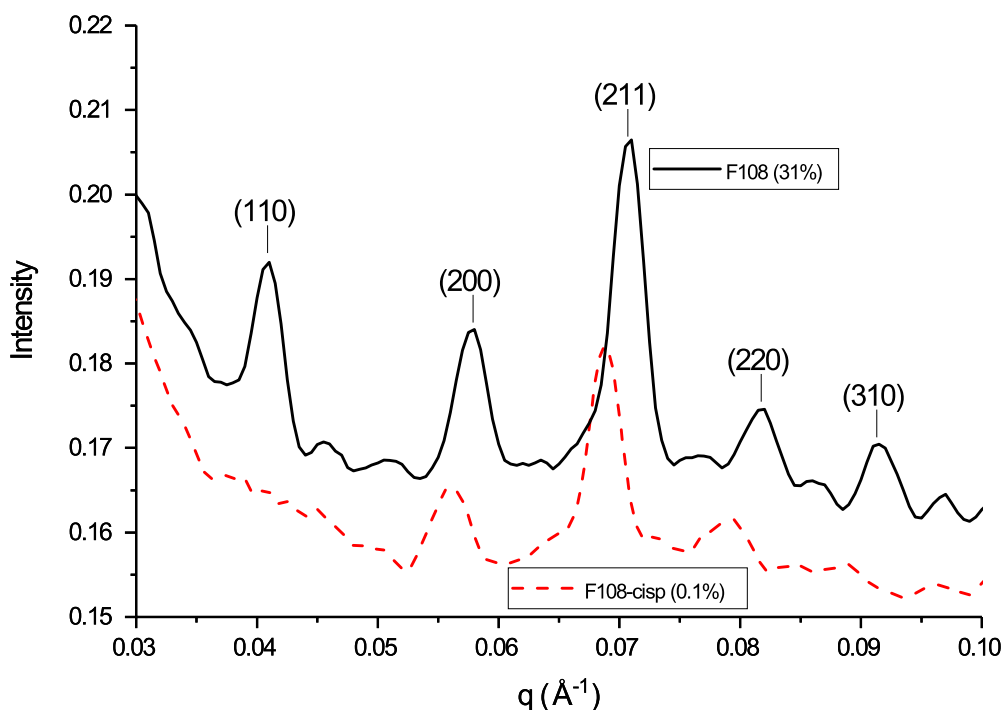
240

241   **Figure 4.** Comparison of peak identifications of neat F108 (31% mass v^{-1}) and F108 mixed
242   cisplatin (0.1% mass v^{-1}) at 28°C.

243

244   Similar to cisplatin mixed P104 at 28°C, cisplatin mixed F108 has the primary peak,

245   (110) at q_0, suppressed significantly. This primary peak suppression was observed previously

246   with dexamethasone and F127 [8] and thin films of poly(alkoxyphenylenevinylene-b-isoprene)

247   rod-coil copolymers arranged into lamellar structures [52]. In this case of F108, the presence of

248   cisplatin reduces the (211) peak (from 0.17:0.21 to 0.16:0.18). Since the higher order peaks are

249   reduced with cisplatin loading and there is evidence of more random scattering, cisplatin is not

250   fully situated within the micelle structure and it is more randomly distributed in solution. This is

251   sensible, since cisplatin is moderately hydrophilic and F108 is 80% hydrophilic, so cisplatin is

252   more distributed throughout the corona and aqueous solution. Maybe there is a saturation of

253   cisplatin within the micelles below 0.1%. Similar to P105, there are also slight shifts to lower q

254   values with added cisplatin for F108 (Table 2), which indicates cisplatin swells F108.

255   Similar to P104 and P105, cisplatin also had little effect on the temperature where

256   ordering occurred relative to the neat F108 samples. Neat F108 ordering was first seen when

257   equilibrated at 22°C , and ~23°C after cisplatin loading. Highest scattering intensity for neat

258   F108 was seen at 30°C, and random scattering was seen at 34°C, evidence of BCC structural

259   breakdown. For cisplatin mixed F108, the same trend was observed. This indicates cisplatin does

260   not stabilize the quasicrystalline lattice in F108 gels.

261   Studies have been carried out to measure the localization of ternary additives with PEO-

262   PPO-PEO micelles [53-57]. Desale et al used an anionic glutamic acid block to coerce cisplatin

263   more to the core-shell interphase separating the hydrophilic and hydrophobic blocks to conjugate

264   and alter the cisplatin binding within the micelle [58]. Based on prior work [18], we believe that

265   the added cisplatin is also localized in the core-shell interphase of the micelles for P104, and

266   P105. The moderate hydrophilicity of cisplatin might help explain the enhanced intensity of

267   structural ordering in P104 and P105, but not in F108.

268   Table 2 shows the identified peak positions for each sample in Figures 1, 3, and 4, and

269   the associated crystal structure identified from peaks present at 28°C. Table 2 also shows the

270   calculated size of each cubic unit cell, a (Å), using equation (1), and the calculated linear thermal

271   expansion coefficient, α_L (^{o}C^{-1}), using equation (6).

272   **Table 2. Fundamental (q_0) and higher order (q_n) peaks (in units of Å^{-1}), identified phase**
273   **structure, fcc (^{a}), bcc (^{b}), unit cell size, a (nm), and linear thermal expansion coefficient, α_L**
274   **(^{o}C^{-1}), at 28°C for neat P104, P105, and F108 (31% mass v^{-1}) and mixed cisplatin (0.02% -**
275   **0.1% mass v^{-1}).**
276

Sample	q_0	q_1	q_2	q_3	q_4	Phase	a(nm)	α_L (^{o}C^{-1})
Neat P104	.0462	.0541^a	.0765^a	.0900^a	-	FCC	**23.2**	**9.7x10^{-3}**
P104-cisp 0.02%	.0463	.0537^a	.0761^a	.0891^a	-	FCC	**23.4**	**8.1x10^{-3}**
P104-cisp 0.04%	.0493	.0555^a	.0785^a	.0918^a	-	FCC	**22.6**	**8.6x10^{-3}**
P104-cisp 0.06%	.0509	.0535^a	.0781^a	.0910^a	-	FCC	**22.7**	**9.0x10^{-3}**
P104-cisp 0.08%	.0492	.0546^a	.0776^a	.0909^a	-	FCC	**22.9**	**9.0x10^{-3}**
P104-cisp 0.1%	.0483	.0556^a	.0787^a	.0925^a	-	FCC	**22.6**	**8.8x10^{-3}**
Neat P105	.0478	.0577^b	.0822^b	.0962^b	-	BCC	**18.7**	**3.8x10^{-3}**
P105-cisp 0.1%	.0470	.0573^b	.0813^b	.0953^b	-	BCC	**18.9**	**4.4x10^{-3}**
Neat F108	.0410	.0578^b	.0709^b	.0820^b	.0913^b	BCC	**21.7**	**1.8x10^{-4}**
F108-cisp 0.1%	.0399	.0565^b	.0691^b	.0790^b	.0890^b	BCC	**22.3**	**1.6x10^{-3}**

277

278   For P104, the neat copolymer and cisplatin mixed copolymer formed fcc phases with

279   identifying peaks (111), (200), (220), and (311) (at q_0, $(4/3)^{1/2}q_0$, $(8/3)^{1/2}q_0$, $(11/3)^{1/2}q_0$,

280   respectively). Santos et al also reported fcc phase structure in the Fm3m space group for 30%,

281   40%, and 34% P104 in 70% H$_2$O, 60% H$_2$O, and 63.4% H$_2$O/2.4% poly(acrylic acid)

282   respectively at 25°C [34]. For P105, the neat copolymer and cisplatin mixed copolymer formed

283   bcc phases with identifying peaks (110), (200), (211), and (220) (at q_0, $2^{1/2}q_0$, $3^{1/2}q_0$ and $2q_0$

284   respectively). Hossain et al also reported bcc phase structure for P105 in the Im3m space group

285   for 39% P105 in 61% water at 25°C. Alexandridis et al, however, observed a primitive phase

286   structure in the Pm3n crystallographic space group for 40%/60% P105/formamide at 30°C [41].

287   For F108, the neat copolymer and cisplatin mixed copolymer formed BCC structures with

288   identifying peaks (110), (200), (211), (220), and (310) (at q_0, $2^{1/2}q_0$, $3^{1/2}q_0$, $2q_0$, and $5^{1/2}q_0$

289   respectively). Quinn et al, however, reported a reversed "double diamond-type" cubic phase,

290   with a Pn3m space group for 0.5 g L^{-1} F108-graphene dispersions at 25°C [46].

291   **Unit cell size.**   The calculated lattice parameter for each sample is listed in Table 2.

292   Cisplatin has a non-systematic effect on the P104 lattice parameter, generally going down with

293   higher concentration. Above 0.4% cisplatin, lattice parameter of the FCC P104 unit cell is

294   reduced by ~2%. This also suggests less water swelling of the PEO block when cisplatin is

295   present. Kayali et al observed a similar trend of decreasing interfacial area per PEO block with

296   increasing copolymer content in P104[30]. Our neat P104 unit cell size is larger than those

297   resolved by Santos et al who calcuated 207 Å for 30% P104/70% H_2O using SAXS [34]. When

298   Santos et al increased P104 to 36%, and mixed with 54% H_2O and 10% poly(acrylic acid)$_{25}$, they

299   saw a more dramatic decrease in unit cell size from 207 Å to 154 Å [34].

300

301   Figure 5 shows the plot of the structure factor peak vs plane designation for neat FCC F108

302   (31% mass v^{-1}) and cisplatin (0.1% mass v^{-1}) mixed F108 at 28°C. The change to a lower slope

303   is indicative of a larger lattice parameter and a swollen structure based on Equation 1.
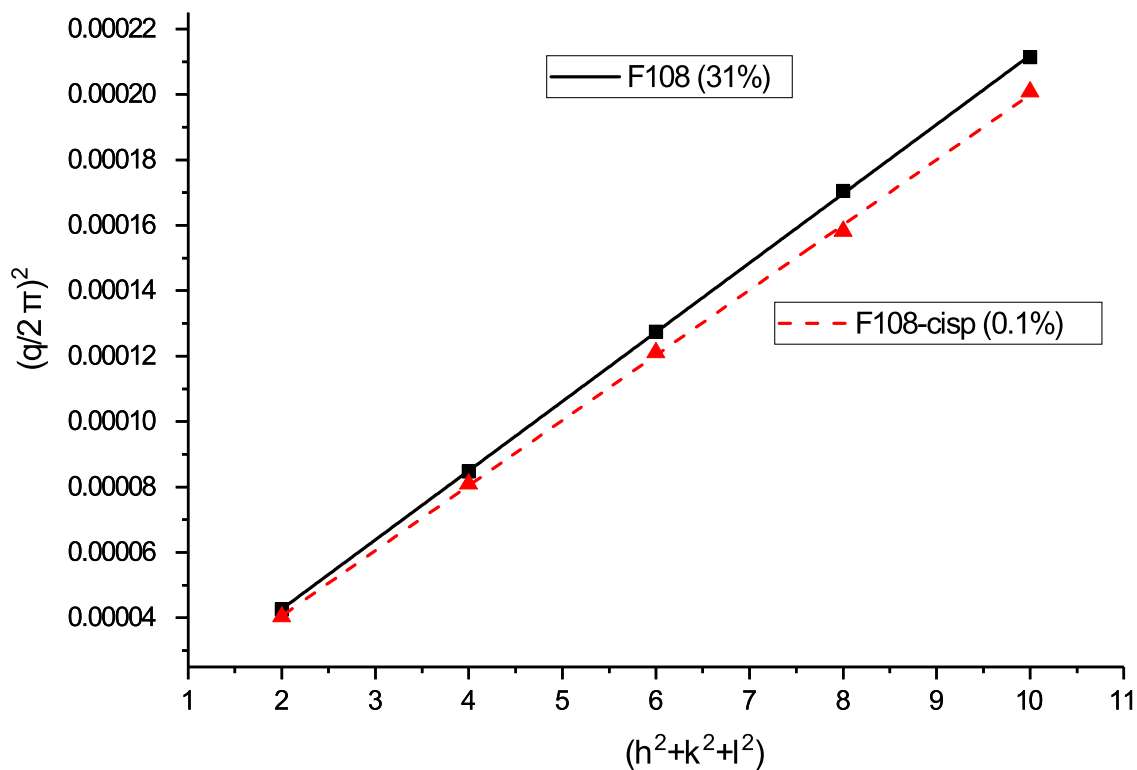
Figure 5. Neat F108 (31% mass v^{-1}) and cisplatin (0.1% mass v^{-1}) mixed F108 unit cell determination $(q/2\pi)^2$ versus $(h^2 + k^2 + l^2)$ from data collected at 28°C.

With added cisplatin, the more hydrophobic P104 unit cell size shrunk, the more amphiphilic P105 saw no change, and the more hydrophilic F108 saw a slight rise in unit cell size, all noted in Table 2

d-spacing and thermal expansion. Figure 6 shows how the distance, d spacing (Å), between adjacent (220) lattice planes for the FCC crystals of neat P104 (31% mass v^{-1}) and cisplatin (0.02%-0.1% mass v^{-1}) mixed P104 with increasing temperature.
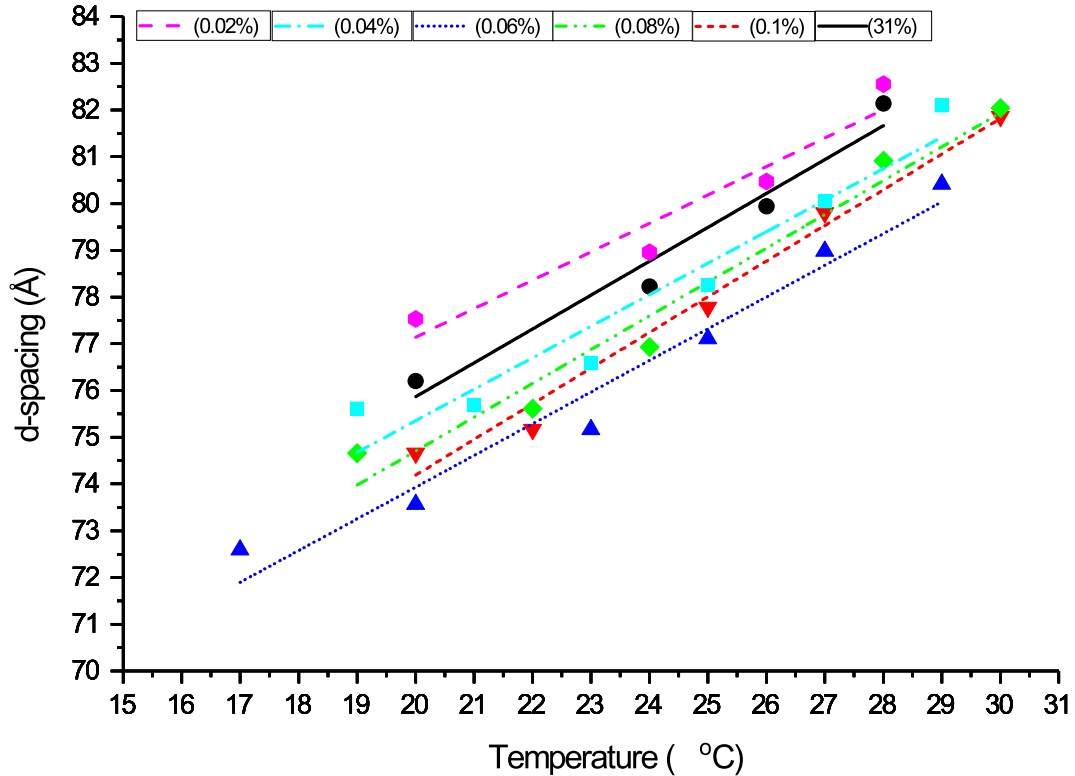
Figure 6. d-spacing (Å) of the (220) plane of neat P104 (31% mass v^{-1}) and cisplatin (0.02%-0.1% mass v^{-1}) mixed P104 with increasing temperature.

All of the P104 formulations increase in lattice d spacing with temperature… they are

expanding, and that could be from the swelling of the PEO blocks with increasing temperature.

These datasets are normally normalized relative to the d spacing itself, so a thermal expansion of

0.7/~70 = ~.01/°C for this specific lattice expansion. This is quite high relative to structural

crystals where expansion is based on the shape of the bond energy diagram of the elements

making up the crystal, or for polymers above Tg, which are typically in the range of 1x10^{-3}/°C. It

326   might be worth backing off and saying that while there is some effect of the cisplatin content on

327   the original d spacing, they all expand at roughly the same rate.

328   Using the data in Figure 6 and equation (6), linear thermal expansion coefficients, α_L,

329   were calculated for neat P104 (31% mass v^{-1}) and cisplatin (0.02%-0.1% mass v^{-1}) mixed P104.

330   Results are shown in Table 2. As expected, all of the colloidal crystals swell with temperature,

331   and the small presence of cisplatin had no pronounced effect on the rate of expansion.

332   As a final comment, the next steps for this analysis will be in confirming the form factor

333   contribution to scattering. We could address a number of questions here without having a

334   confirmed form factor solution under all cases. Continuing in this vein should raise the

335   confidence in the overall analysis.

336

337   **4. Conclusions**:
338
339   SAXS analysis of P104, P105, and F108 solutions also containing cisplatin has revealed

340   several key changes in their phase behavior relative to neat systems. First, P104 formed BCC

341   structures while P105 and F108 formed FCC crystals that were not transformed into a new

342   structure by adding cisplatin. For P104 and P105, cisplatin enhances the structural ordering with

343   sharper peaks at the same compared to the neat samples tested at the same temperature.

344   Unexpectedly, F108 showed the opposite effect as the intensity decreased with added cisplatin

345   indicating more disorder. We found a little evidence to suggest that the presence of cisplatin

346   helps coerce ordering of P104 as it formed crystals at slightly lower temperature and remaining

347   at slightly higher temperatures than the neat crystals, but it apparently adds to the structural

348   disorder in F108, a more hydrophilic colloidal crystal.

349   The presence of cisplatin stabilized the quasicrystalline lattice in P104 and P105 gels,

350   evidenced by the preservation of ordered phases and high scattering intensities at 30°C for

351   cisplatin mixed copolymers, but much lower scattering intensities at 30°C for neat copolymers.

352   The P104 crystals that formed with cisplatin tended to have smaller lattice parameters (2-3%)

353   than the neat systems while the other formulations tended to swell upon interacting with

354   cisplatin. This was measurable but perhaps not statistically significant. The linear thermal

355   expansion coefficient for neat P104 was $9.7 \times 10^{-3} \text{°C}^{-1}$, and other cisplatin-loaded gels expanded at

356   similar rates, an order of magnitude higher in response than for bulk polymers above Tg

357   undergoing thermal expansion. We also report on the thermal expansion of cisplatin loaded and

358   neat P105 and F108 mixtures with less fidelity, in part due to the limited analysis time at

359   Argonne.

360   These experiments show how using SAXS coupled with a dynamic heating protocol,

361   structural changes in P104, P105, and F108 amphiphilic copolymer solutions (31% mass v^{-1}) can

362   be characterized when formulated with cisplatin (0.02% to 0.1% mass v^{-1}). We have shown that

363   the evolution of the FCC or BCC phase in PEO-PPO-PEO solutions follow a nucleation and

364   growth mechanism over a range of temperatures (10°C to 35°C). For cisplatin, understanding

365   where a chemotherapeutic molecule resides in a structure may affect its overall bioavailability,

366   and these early experiments help to suggest at least how cisplatin is interacting within the

367   evolving structure of a colloidal crystal.

368

374

References:

1. Wanka G, Hoffmann H, Ulbricht W. Phase diagrams and aggregation behavior of poly(oxyethylene)-poly(oxypropylene)-poly(oxyethlene) triblock copolymers in aqueous solutions. Macromolecules. 1994;27:4145-59.

2. Alexandridis P, Navaggioli T, Hatton TA. Temperature effects on structural properties of pluronic P104 and F108 PEO-PPO-PEO block copolymer solutions. Langmuir. 1995;11:1468-76.

3. Alexandridis P, Holzwarth JF, Hatton TA. Micellization of poly (ethylene oxide)-poly (propylene oxide)-poly (ethylene oxide) triblock copolymers in aqueous solutions: thermodynamics of copolymer association. Macromolecules. 1994;27(9):2414-25.

4. Sharma PK, Bhatia SR. Effect of anti-inflammatories on Pluronic® F127: micellar assembly, gelation and partitioning. International Journal of Pharmaceutics. 2004;278(2):361-77. doi:10.1016/j.ijpharm.2004.03.029.

5. Sharma PK, Reilly MJ, Bhatia SK, Sakhitab N, Archambault JD, Bhatia SR. Effect of pharmaceuticals on thermoreversible gelation of PEO–PPO–PEO copolymers. Colloids and Surfaces B: Biointerfaces. 2008;63(2):229-35. doi:10.1016/j.colsurfb.2007.12.009.

6. Sharma PK, Reilly MJ, Jones DN, Robinson PM, Bhatia SR. The effect of pharmaceuticals on the nanoscale structure of PEO–PPO–PEO micelles. Colloids and Surfaces B: Biointerfaces. 2008;61(1):53-60.

7. Bouchemal K, Agnely F, Koffi A, Ponchel G. A concise analysis of the effect of temperature and propanediol-1, 2 on Pluronic F127 micellization using isothermal titration microcalorimetry. Journal of Colloid And Interface Science. 2009;338(1):169-76. doi:10.1016/j.jcis.2009.05.075.

8. Meznarich NAK, Juggernauth KA, Batzli KM, Love BJ. Structural changes in PEO–PPO–PEO gels induced by methylparaben and dexamethasone observed using time-resolved SAXS. Macromolecules. 2011;44(19):7792-8. doi:10.1021/ma2015358.

9. Meznarich NAK, Love BJ. The kinetics of gel formation for PEO−PPO−PEO triblock copolymer solutions and the effects of added methylparaben. Macromolecules. 2011;44(9):3548-55. doi:10.1021/ma200302s.

10. Lam Y-M, Goldbeck-Wood G. Mesoscale simulation of block copolymers in aqueous solution: parameterisation, micelle growth kinetics and the effect of temperature and concentration morphology. Polymer. 2003;44:3593-605.

11. Barba AA, d'Amore M, Grassi M, Chirico S, Lamberti G, Titomanlio G. Invenstigation of pluronic F127-water solutions phase transitions by DSC and dielectric spectroscopy. Journal of Applied Polymer Science. 2009;114:688-95.

12. Nalbandian RM, Henry RL, Balko KW, Adams DV, Neuman NR. Pluronic F-127 gel preparation as an artificial skin in the treatment of third-degree burns in pigs. Journal of Biomedical Materials Research. 1987;21:1135-48.

13. Hsu S-H, Leu Y-L, Hu J-W, Fang J-Y. Physiochemical characterization and drug release of thermosensitive hydrogels composed of a hyaluronic acid/pluronic F127 graft. Chemical and Pharmaceutical Bulletin. 2009;57(5):453-8.

14. Kabanov A, Zhu J, Alakhov V. Pluronic block copolymers for gene delivery. Advances in Genetics. 2005;53:231-61.

15. Ohta S, Nitta N, Takahashi M, Sonoda A, Tanaka T, Yamasaki M, Furukawa A, Takazakura R, Murata K, Sakamoto T, Kushibiki T, Tabata Y. Pluronic F127: Application in arterial embolization. Journal of Vascular and Interventional Radiology. 2006;17:533-9.

16. Escobar-Chavez JJ, Lopez-Cervantes M, Naik A, Kalia YN, Quintanar-Guerrero D, Ganem-Quintanar A. Applications of thermo-reversible pluronic F-127 gels in pharmaceutical formulations. Journal of Pharmacy & Pharmaceutical Sciences. 2006;9(3):339-58.

17. Thompson AL, Love BJ. Thermodynamic properties of aqueous PEO-PPO-PEO micelles with added methylparaben determined by differential scanning calorimetry. Journal of Colloid And Interface Science. 2013;398:270-2. doi:10.1016/j.jcis.2013.01.064.

18. Thompson AL, Love BJ. Thermodynamic properties of aqueous PEO-PPO-PEO micelles of varying hydrophilicity with added cisplatin determined by differential scanning calorimetry. Journal of Thermal Analysis and Calorimetry. 2016;127(2):1583-92.

19. Mortensen K, Batsberg W, Hvidt S. Effects of PEO-PPO diblock impurities on the cubic strucutre of aqueous PEO-PPO-PEO pluronics micelles: fcc and bcc ordered structures in F127. Macromolecules. 2008;41:1720-7.

20. Mortensen K, Pedersen JS. Structural study on the micelle formation of poly(ethylene oxide)-poly(propylene oxide)-poly(ethylene oxide) triblock copolymer in aqueous solution. Macromolecules. 1993;26:805-12.

21. Wolff M, Magerl A, Zabel H. NS-SANS for the investigation of micellar systems. Thin Solid Films. 2007;515:5724-7.

429   22. Prud'homme RK, Wu G, Schneider DK. Structure and rheology studies of poly(oxyethylene-oxypropylene-
430   oxyethylene) aqueous solution. Langmuir. 1996;12:4651-9.
431   23. Svensson B, Olsson U, Alexandridis P, Mortensen K. A SANS investigation of reverse (water-in-oil) micelles of
432   amphiphilic block copolymers. Macromolecules. 1999;32:6725-33.
433   24. Lazzara G, Milioto S, Gradzielski M. The solubilisation behavior of some dichloroalkanes in aqueous solutions
434   of PEO-PPO-PEO triblock copolymers: a dynamic light scattering, fluorescence spectroscopy, and SANS study.
435   Physical Chemistry Chemical Physics. 2006;8:2299-312.
436   25. Khimani M, Ganguly R, Aswal VK, Nath S, Bahadur P. Solubilization of parabens in aqueous pluronic
437   solutions: investigating the micellar growth and interaction as a function of paraben composition. The Journal of
438   Physical Chemistry B. 2012;116:14943-50.
439   26. Khimani M, Verma G, Kumar S, Hassan PA, Aswal VK, Bahadur P. pH induced tuning of size, charge and
440   viscoelastic behavior of aqueous micellar solution of Pluronic® P104-anthranilic acid mixtures: a scattering,
441   rheology, and NMR study. Colloids and Surfaces A: Physicochemical and Engineering Aspects. 2015;470:202-10.
442   27. Chen S-H, Liao C, Fratini E, Baglioni P, Mallamace F. Interaction, critical, percolation and kinetic glass
443   transitions in pluronic L-64 micellar solutions. Colloids and Surfaces A: Physicochemical and Engineering Aspects.
444   2001;183-185:95-111.
445   28. Liu Y, Chen S-H, Huang JS. Small-angle neutron scattering analysis of the structure and interaction of triblock
446   copolymer micelles in aqueous solution. Macromolecules. 1998;31:2236-44.
447   29. Svensson B, Alexandridis P, Olsson U. Self-assembly of a poly(ethylene oxide)/poly(propylene oxide) block
448   copolymer (pluronic P104, $(EO)_{27}(PO)_{61}(EO)_{27}$) in the presence of water and xylene. The Journal of Physical
449   Chemistry B. 1998;102:7541-8.
450   30. Kayali I, Khan A, Lindman B. Solubilization and location of phenethylalcohol, benzaldehyde, and limonene in
451   lamellar liquid crystal formed with block copolymer and water. Journal of Colloid And Interface Science.
452   2006;297:792-6.
453   31. Hamley IW, Castelletto V, Ricardo NM, Pinho ME, Booth C, Attwood D, Yang Z. A SAXS study of the
454   structure of gels formed by mixtures of polyoxyalkylene triblock copolymers. Polymer International. 2007;56:88-92.
455   32. Zhang J, Han B, Zhao Y, Li J, Yang G. Switching micellization of pluronics in water by CO_2. Chemistry a
456   European Journal. 2011;17:4266-72.
457   33. Zhang R, Liu J, He J, Han B, Liu Z, Jiang T, Wu W, Rong L, Zhao H, Dong B, Hu G-H. Compressed ethylene-
458   assisted formation of the reverse micelle of PEO-PPO-PEO copolymer. Macromolecules. 2003;36:1289-94.
459   34. Santos Sd, Luigjes B, Piculell L. Associative phase behavior and disintegration of copolymer aggregates on
460   adding poly(acrylic acid) to aqueous solutions of a PEO-PPO-PEO triblock copolymer. Soft Matter. 2010;6:4756-
461   67.
462   35. Cui X, Moon S-W, Zin W-C. High-yield synthesis of monodispersed SBA-15 equilateral hexagonal platelet with
463   thick wall. Materials Letters. 2006;60:3857-60.
464   36. Zhou D, Alexandridis P, Khan A. Self-assembly in a mixture of two poly(ethylene oxide)-b-poly(propylene
465   oxide)-b-poly (ethylene oxide) copolymers in water. Journal of Colloid And Interface Science. 1996;183:339-50.
466   37. Baldrian J, Steinhart M, Amenitsch H, Bernstorff S. Disorder-order-crystalline state transitions of PEO-b-PPO-
467   b-PEO copolymers and their blends: SAXS/WAXS/DSC study. Journal of Macromolecular Science®, Part B:
468   Physics. 2009;48:174-84.
469   38. Aramaki K, Hossain MK, Rodriguez C, Uddin MH, Kunieda H. Miscibility of block copolymers and surfactants
470   in lamellar liquid crystals. Macromolecules. 2003;36:9443-50.
471   39. Hossain MK, Hinata S, Lopez-Quintela A, Kunieda H. Phase behavior of poly(oxyethylene)-
472   poly(oxypropylene)-poly(oxyethylene) block copolymer in water and water-$C_{12}EO_5$ Systems. Journal of Dispersion
473   Science and Technology. 2003;24(3):411-22.
474   40. Alexandridis P, Zhou D, Khan A. Lyotropic liquid crystallinity in amphiphilic block copolymers: temperature
475   effects on phase behavior and structure for poly(ethylene oxide)-b-poly(propylene oxide)-b-poly(ethylene oxide)
476   copolymers of different composition. Langmuir. 1996;12:2690-700.
477   41. Alexandridis P. Structural polymorphism of poly(ethylene oxide)-poly(propylene oxide) block copolymers in
478   nonaqueous polar solvents. Macromolecules. 1998;31:6935-42.
479   42. Li J, Tang H, Chen L, Chen R, Pan M, Jiang SP. Highly ordered and periodic mesoporous nafion membranes via
480   colloidal silica mediated self-assembly for fuel cells. Chemical Communications - Royal Society of Chemistry.
481   2013;49:6537-9.
482   43. Lu J, Tang H, Xu C, Jiang SP. Nafion membranes with ordered mesoporous structre and high water retention
483   properties for fuel cell applications. Journal of Materials Chemistry. 2012;22:5810-9.

484   44. Nambam JS, Philip J. Thermogelling properties of triblock copolymers in the presence of hydrophilic Fe_3O_4
485   nanoparticles and surfactants. Langmuir. 2012;28:12044-53.
486   45. Shih K-C, Li C-Y, Li W-H, Lai H-M. Fine structures of self-assembled beta-cyclodextrin/Pluronic in dilute and
487   dense systems: a small angle X-ray scattering study. Soft Matter. 2014;10:7606-14.
488   46. Quinn MDJ, Du J, Boyd BJ, Hawley A, Notley SM. Lipid liquid-crystal phase change induced through a near-
489   infrared irradiation of entrained graphene particles. Langmuir. 2015;31:6605-9.
490   47. Hartnett TE, Ladewig K, O'Connor AJ, Hartley PG, McLean KM. Physicochemical and cytotoxicity analysis of
491   glycerol monoolein-based nanoparticles. RSC Advances. 2015;5:26543-9.
492   48. Tirumala VR, Romang A, Agarwal S, Lin EK, Watkins JJ. Well ordered polymer melts from blends of
493   disordered triblock copolymer surfactants and functional homopolymers**. Advanced Materials. 2008;20:1603-8.
494   49. Li Y, Keilbach A, Mizoshita N, Inagaki S, Bein T. Formation of hexagonal and cubic fluorescent periodic
495   mesoporous organosilicas in the channels of anodic alumina membranes. Journal of materials Chemistry C.
496   2014;2:50-5.
497   50. Lin Y, Daga VK, Anderson ER, Gido SP, Watkins JJ. Nanoparticle-driven assembly of block copolymers: a
498   simple route to ordered hybrid materials. Journal of the American Chemical Society. 2011;133:6513-6.
499   51. Schmolka IR. Artificial skin I. preparation and properties of pluronic F-127 gels for treatment of burns. Journal
500   of Biomedical Materials Research. 1972;6:571-82.
501   52. Olsen BD, Li X, Wang J, Segalman RA. Near-surface and internal lamellar structure and orientation in thin films
502   of rod-coil block copolymers. Soft Matter. 2009;5:182-92.
503   53. Nagarajan R. Solubilzation of hydrocarbons and resulting aggregate shape transitions in aqueous solutions of
504   Pluronic® (PEO-PPO-PEO) block copolymers. Colloids and Surfaces B: Biointerfaces. 1999;16:55-72.
505   54. Nagarajan R. Solubilization of "guest" molecules into polymeric aggregates. Polymers for Advanced
506   Technologies. 2001;12:23-43.
507   55. Steinbeck CA, Hedin N, Chmelka BF. Interactions of Charged Porphyrins with Nonionic Triblock Copolymer
508   Hosts in Aqueous Solutions. Langmuir. 2004;20:10399-412.
509   56. Jia L, Guo C, Yang L, Xiang J, Tang Y, Liu H. Interaction between reduced glutathione and PEO-PPO-PEO
510   copolymers in aqueous solutions: studied by ^{1}H NMR and spin-lattice relaxation. The Journal of Physical
511   Chemistry. 2011;115:2228-33.
512   57. Ruthstein S, Raitsimring AM, Bitton R, Frydman V. Distribution of guest molecules in pluronic micelles studied
513   by double electron electron spin resonance and small angle X-ray scattering. Physical Chemistry Chemical Physics.
514   2009;11:148-60.
515   58. Desale SS, Cohen SM, Zhao Y, Kabanov AV, Bronich TK. Biodegradable hybrid polymer micelles for
516   combination drug therapy in ovarian cancer. Journal of Controlled Release. 2013;171:339-48.

517